Very slow expansion of an ultracold plasma formed in a seeded supersonic molecular beam of NO

J. P. Morrison, C. J. Rennick, and E. R. Grant*
Department of Chemistry, University of British Columbia, Vancouver British Columbia, Canada V6T 1Z1
(Received 21 December 2008; published 9 June 2009)

The double-resonant laser excitation of nitric oxide, cooled to 1 K in a seeded supersonic molecular beam, yields a gas of $\approx 10^{12}$ molecules per cubic centimeter in a single selected Rydberg state. This population evolves to produce prompt free electrons, and a durable cold plasma of electrons and intact NO^+ ions. This plasma travels with the molecular beam through a field-free region to encounter a grid. The atomic weight of the expansion gas controls the beam velocity and hence the flight time from the interaction region to the grid. Monitoring electron production as the plasma traverses this grid measures its longitudinal width as a function of flight time. Comparing these widths to the width of the laser beam that defines the initial size of the illuminated volume allows us to gauge the rate of expansion of the plasma. We find that the plasma created from the evolution of a Rydberg gas of NO expands at a small but measurable rate, and that this rate of expansion accords with the Vlasov equations for an initial electron temperature of $T_e \approx 7$ K.

DOI: 10.1103/PhysRevA.79.062706 PACS number(s): 34.80.Lx, 52.55.Dy, 32.80.Ee, 33.80.Gj

I. INTRODUCTION

When a tunable pulsed laser promotes a substantial fraction of the atoms held in a magneto-optical trap (MOT) to a high-Rydberg state ($n > 30$), the ensemble spontaneously evolves on a microsecond time scale to produce an ultracold plasma [1–6]. This phenomenon and the plasma that it forms have attracted a great deal of recent attention [7–9] because these rarified laboratory systems can display a degree of charged-particle correlation otherwise found only in thermonuclear explosions and the cores of dense stars.

Coulomb interactions act to govern the dynamics of the charged particles in a plasma when their electrostatic repulsion exceeds their thermal translational energy. The point at which this occurs depends on the density and temperature of the plasma [10]. The parameter, Γ, gauges the degree of correlation in terms of the dimensionless ratio,

$$\Gamma = \frac{e^2/4\pi\varepsilon_0 a}{kT}, \tag{1}$$

where e is the charge, and a, the Wigner-Seitz radius, relates to the particle density, ρ, by

$$4/3\pi a^3 = 1/\rho. \tag{2}$$

Conditions under which Γ substantially exceeds one can give rise to liquidlike or solidlike spatial correlations, leading ultimately to Coulomb crystallization and a quantum-state-detailed variant of the Mott insulator-to-metal phase transition [11].

Ultracold plasmas formed in MOTs at densities of the order of 10^{10} atoms per cubic centimeter have an initial Wigner-Seitz radius of $a = 3$ μm. This average interparticle spacing grows with plasma expansion at rates that fit with a decline in electron temperature from tens of kelvins to the order of 10 K [12]. At its maximum sometime during the 40 μs observation window, these conditions give rise to electron correlation parameters in the range of $\Gamma_e \approx 0.1$.

Recently, we have demonstrated the evolution to an ultracold plasma by NO molecules entrained in a supersonic expansion [13]. This development holds interesting potential for the study of correlation in mesoscopic charged-particle ensembles. The use of supersonic expansions substantially broadens the scope of systems that can be studied; any substance that can be volatilized—including large molecules and refractory metal clusters—can be entrained in a seeded supersonic molecular beam. Heavy-particle internal degrees of freedom present new dimensions for plasma relaxation dynamics, including an accommodation of electron energy in ion degrees of freedom extending beyond the translational heat capacity to include rotational, and in some cases vibrational and vibronic, states.

In our experiment, a seeded supersonic expansion provides NO at a local density of 5×10^{13} molecules per cubic centimeter and a moving-frame translational temperature of less than 1 K, determined simply by the backing pressure and nozzle diameter of the source, and the distance downstream to the interaction region. Saturated steps of double-resonant laser excitation promote about 10% of these molecules to a selected high-Rydberg state, from which they evolve to form a remarkably durable ultracold plasma. At the Wigner-Seitz radius corresponding to this density ($a \approx 400$ nm), an electron temperature of 10 K would yield a correlation, $\Gamma_e \approx 4$.

Our initial observations provide no direct means to quantify the ion or electron temperatures in the fully formed plasma. We do, however, know that the plasma expands very little during the 9 μs observational window of those experiments.

We have now more than tripled this observation time. Replacing helium with neon, argon, and krypton as expansion gases into which we seed NO, we have reduced the beam velocity to substantially increase the flight time in the field-free region of our apparatus. By monitoring electron production as the plasma traverses the grid that defines the

*Author to whom correspondence should be addressed; edgrant@chem.ubc.ca

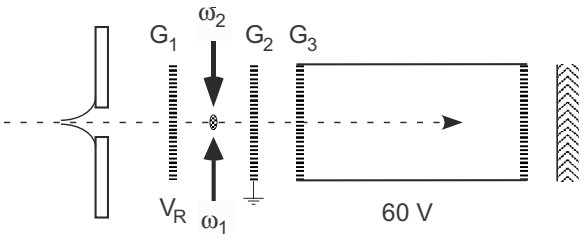

FIG. 1. Schematic diagram showing the path of the molecular beam from a differentially pumped source chamber to the interaction region through a skimmer entering a system of three grids ending in a flight tube capped by a microchannel plate detector. Drawn to approximate scale with a G_1 to G_2 spacing of 2 cm.

end of the field-free region, we measure the longitudinal width of this distribution of NO^+ ions and electrons as a function of flight times from 9 to 30 μs.

Comparing these widths to the width of the laser beam that defines the initial size of the illuminated volume, we are now much better able to gauge the rate of expansion of the plasma. We find that the plasma created in a molecular beam from a Rydberg gas of NO does expand at a small but measurable rate, and that this rate of expansion accords with the Vlasov equations for an initial electron temperature of $T_e \approx 7$ K.

II. EXPERIMENTAL

A pulsed jet of NO, seeded nominally at 10% in He, Ne, Ar, or Kr at a backing pressure of 5 atm, expands through the 0.5-mm-diameter nozzle of a Series 9 pulse valve (Parker Hannifin). 2 cm downstream, the free jet passes through an electroformed Ni skimmer to enter a mu-metal shielded electron spectrometer as a 1–mm-diameter differentially pumped supersonic molecular beam.

Figure 1 diagrams our two-stage electron spectrometer. In the first stage, a pair of grounded grids, G_1 and G_2, held perpendicular to the axis of the molecular beam, define a field-free laser-molecular-beam interaction region. Tunable pulses from two frequency-doubled Nd:yttrium aluminum garnet-pumped dye lasers overlap to intersect the molecular beam halfway between the plates.

Here, NO molecules absorb light in two resonant steps to reach a selected high-Rydberg state. These high-Rydberg NO molecules interact to form a plasma. This plasma volume moves with the velocity of the molecular beam to traverse G_2, at which point it encounters a 60 V cm^{-1} field. This field gradient extracts and accelerates plasma electrons to a multichannel plate detector. On the time scale of our measurement, electrons extracted at G_2 appear instantaneously at the detector, and the profile of this signal thus integrates transverse slices of the electron-density distribution of the plasma as it passes through G_2.

Figure 2 shows an energy diagram for the excitation of NO. An initial laser pulse (ω_1) pumps the transition from the ground, $X\ ^2\Pi$, state to rotational substates of the $v=0$ vibrational level of the first electronically excited state, $^2\Sigma^+$. A second laser (ω_2), timed to coincide with ω_1, excites from a

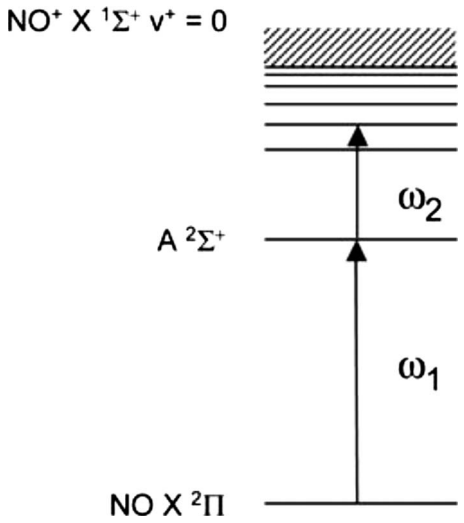

FIG. 2. Excitation scheme for the population of nf Rydberg states by double-resonant transitions via the $^2\Sigma^+$, $v=0$, $N=0$, $J=\frac{1}{2}(+)$ state of NO.

chosen level in this gateway system to a selected high-Rydberg state situated below the lowest ionization threshold.

At high laser-pulse energies two-photon absorption of ω_1 alone ionizes NO. Monitoring the electron signal as a function of the ω_1 wavelength under these conditions produces a rotationally resolved resonant ionization spectrum of the $v=0$ band of the $^2\Sigma^+$ state. We analyze the intensities of lines in this spectrum to estimate the rotational temperature of NO under our expansion conditions.

For plasma experiments, we attenuate ω_1 using a pair of Glan-Taylor polarizing prisms to eliminate any background signal from ω_1 alone, and then counterpropagate unfocused ω_1 and ω_2 laser beams to intersect the molecular beam as indicated in Fig. 1. This illumination geometry crosses a cylindrical photon field with a collimated molecular beam to produce a prolate-ellipsoid excitation volume that propagates sideways with the velocity of the beam toward G_2. The diameter of ω_1 at its intersection with the molecular beam determines the initial equatorial width of this ellipsoid.

We experimentally gauge this limiting laser spot size by tracing the integrated intensity of ω_1 as a function of the position of a razor blade scanned through the beam waist at a distance corresponding to the point at which the laser pulse crosses the axis of the molecular beam. This measurement yields a value of 758 μm for the width of the active excitation volume along the propagation axis of the beam. The divergence of the molecular beam after the skimmer determines a cross-beam length for this illuminated cylinder of approximately 5 mm.

III. RESULTS

The supersonic expansion of an ideal monatomic gas under the present conditions of backing pressure nozzle diameter cools to a parallel temperature, $T_\parallel^\infty$, of about 700 mK, where $T_\parallel^\infty$ represents the second moment of the velocity distribution function along the axis of the molecular beam [14].

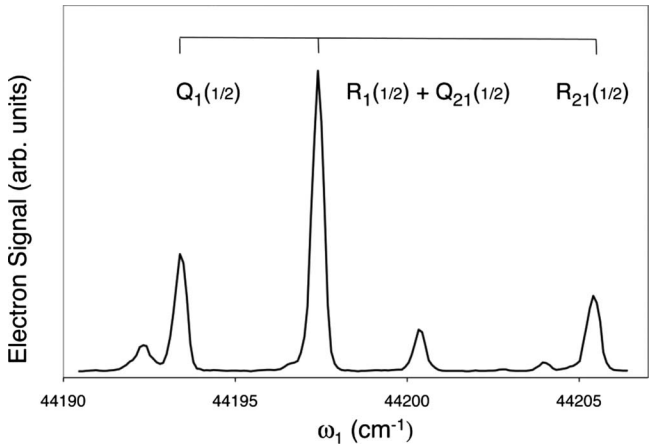

FIG. 3. Resonant 1+1 ionization spectrum of the $X\ ^2\Pi(v''=0)$ to $A\ ^2\Sigma^+(v'=0)$ transition in NO seeded 1:10 in a supersonic beam of He. This pattern of intensities fits a ground-state population distribution corresponding to a rotational temperature, $T_R^\infty=2.5$ K.

A molecule seeded in such an expansion cools to the moving-frame translational temperature of the carrier gas. Supersonic expansion cools molecular rotation as well but the cross section for rotational relaxation is smaller than that for translation. As a result, when collisions cease, the terminal rotational temperature, T_R^∞, exceeds $T_\parallel^\infty$. Figure 3 shows a ω_1 scan of the resonant ionization spectrum of the $X\ ^2\Pi(v''=0)$ to $A\ ^2\Sigma^+(v'=0)$ transition of NO seeded in He, from which we estimate $T_R^\infty=2.5$ K. Expansions in Ne, Ar, and Kr yield the same rotational temperatures.

Our experiment at present provides no direct means to measure the absolute density of excited NO molecules in the active excitation volume. It is nevertheless straightforward to calculate an upper limit. From the nozzle diameter and backing pressure, we estimate the centerline density of particles in the molecular beam to be 4.8×10^{14} cm^{-3} [13,15]. The seeding ratio of NO is 0.1. At a rotational temperature of 3 K, 87% of these molecules populate the two parity components of the rotational ground state. Two saturated steps of laser excitation transfer 12.5% of this population to a parity-selected high-Rydberg state. In combination, these factors predict the density of excited NO molecules available for plasma formation to be 5×10^{12}cm^{-3}.

Various experimental causes could combine to reduce this number in practice. Incomplete opening of the pulsed nozzle could limit flow, reducing the density of the molecular beam. Laser beam intensity inhomogeneities could give rise to regions of the active volume in which the first or second steps in the excitation sequence fail to saturate. However, we routinely optimize the nozzle to maximize the throughput, and adjust the laser power and alignment to maximize signal. These experimental procedures provide some basis for confidence in the above figure as an estimate for the density of excited NO molecules on the axis of the molecular beam. Off the axis of the beam and away from the most intense core of the overlapped laser beams, the density of excited NO molecules is certain to be lower as is the charged-particle density of the corresponding plasma. For illustrative purposes, calculations below will make reference to the upper-limiting centerline concentration of excited NO that defines the region of peak plasma density.

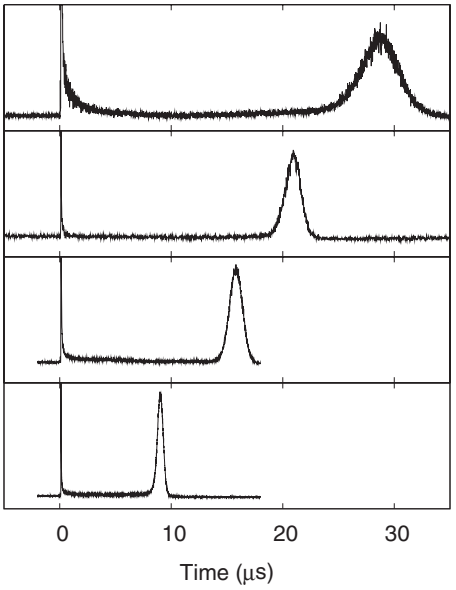

FIG. 4. Electron signal waveforms appearing at G_2 following the substantial promotion of NO molecules to the $52f(2)$ Rydberg state in seeded supersonic expansions of He, Ne, Ar, and Kr (from bottom to top) using the experimental flight path diagrammed in Fig. 1.

To prepare a nitric oxide plasma, we set the frequency of ω_1 on the $Q_1(\frac{1}{2})$ line of the X-A system $[X\ ^2\Pi v''=0,\ N''=1,\ J''=\frac{1}{2}(-)$ to $A\ ^2\Sigma^+v'=0,\ N'=0,\ J'=\frac{1}{2}(+)]$, and tune ω_2 so that the total $\omega_1+\omega_2$ energy approaches the adiabatic ionization threshold of NO. Figure 4 shows electron-signal waveforms obtained for expansions of NO in He, Ne, and Ar, consisting of a prompt electron signal that appears within a few nanoseconds of ω_2 followed tens of microseconds later by a broader late signal.

In previous work, we have established that these waveforms reflect the production of an ultracold plasma of electrons and molecular nitric oxide cations [13]. The prompt signal arises from electrons released early in the formation of the plasma. The late signal marks the passage of the quasineutral plasma through the grid G_2 at the laboratory velocity of the molecular beam.

Gating on the late signal and scanning the wavelength of ω_2, we obtain a spectrum of closely spaced resonances, which is shown for a backing gas of Ar in Fig. 5. We assign this spectrum to lines in the $nf(2)$ Rydberg series [16], where the number 2 refers to the rotational level of NO^+ to which the series converges. The time traces shown in Fig. 4 are obtained for ω_2 tuned to $52f(2)$. We observe very similar spectra and absolute intensities for He and Ne. Expansion in Kr reduces the late-peak intensity by about a factor of four. We are not able to form a plasma from NO expanded in Xe.

For each expansion gas, the measured arrival time of the plasma at G_2, coupled with the known flight distance from the laser interaction region, yields a sharply defined laboratory-frame average velocity $\langle v_z\rangle$ by which to convert the observed temporal width to a spatial width along the propagation axis of the molecular beam. Figure 6 plots the

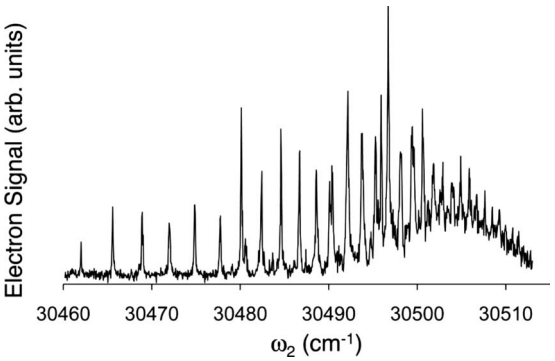

FIG. 5. Resonances in the late signal observed scanning ω_2 for the plasma formed from NO seeded in Ar. Spectrum assigned to lines in the *nf* Rydberg series converging to the rotational level $N^+=2$ in the vibrational ground state of $NO^+X\ ^1\Sigma^+$. $52f(2)$ falls at an ω_2 energy of 30 493.9 cm^{-1}, with a convergence limit of 30 534.5 cm^{-1}.

late-peak waveforms from Fig. 4 that are transformed to distance. We interpret these growing widths to represent the plasma density distribution as it expands in the spatial dimensions transverse to the laser illumination axis. Distances measured in the z dimension fit well with a representation of this expansion in terms of a two-dimensional Gaussian:

$$n_i(y,z,t) = \frac{N_i}{\sigma(t)\sqrt{2\pi}} \exp\left[\frac{-(y^2+z^2)}{2\sigma^2(t)}\right], \tag{3}$$

for which $\Gamma = 2\sqrt{2\ln 2}\sigma(t)$ defines the full width at half maximum (FWHM) of the plasma density distribution in

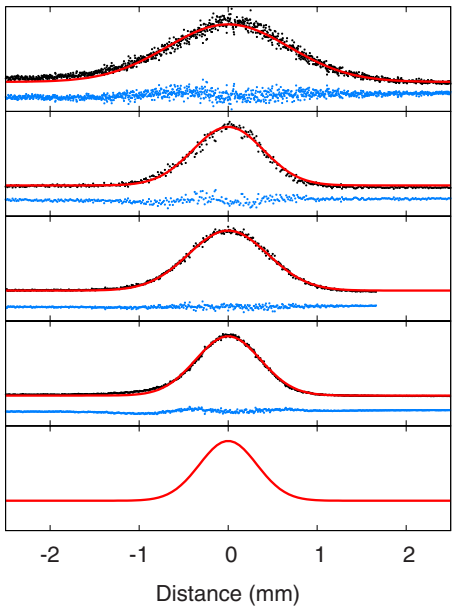

FIG. 6. (Color online) Late electron-signal temporal waveforms from Fig. 4 transformed to yield spatial plasma distributions, displayed according to peak arrival time at G_2. Solid curves show Gaussian fits with residuals below. The bottom figure is derived from the measurement of laser width, above which are plotted the data for He, Ne, Ar, and Kr carrier gases.

TABLE I. Arrival times, estimated velocities, and widths obtained by fitting Gaussian distributions to the spatial waveforms pictured in Fig. 6, as transformed from the flight-time-dependent electron signals shown in Fig. 4.

Carrier gas	Arrival time (μs)	Velocity (ms^{-1})	$\sigma(t)$ (μm)	Width (μm)
He	9.0	1358	364	856
Ne	15.8	758	446	1050
Ar	20.1	560	548	1291
Kr	28.7	394	686	1617

space, as defined by the time-varying standard deviation, $\sigma(t)$. Table I lists the arrival times and spatial widths of the electron-density images obtained in this way for all four expansion gases used in this study.

IV. DISCUSSION

By choice of the expansion gas, we systematically vary the laboratory velocity of nitric oxide in a differentially pumped seeded supersonic molecular beam. Crossing this beam with the output of two dye lasers, we use double-resonant excitation to transform a prolate volume element with a minor axis diameter smaller than 1 mm into a dense distribution of NO molecules excited to a selected high-Rydberg state substantially below the lowest ionization threshold.

This population of high-Rydberg molecules evolves to form a plasma of NO^+ cations and electrons. The volume element containing this plasma moves through a field-free region with the propagation velocity of the molecular beam to traverse a perpendicular grid and enter a 60 V/cm field gradient. Transmission of this volume element through the grid disrupts the plasma to produce a waveform of promptly detected electrons that maps the plasma charge-density distribution along the axis of the molecular beam.

Converting these temporal images to displacements in space, we measure the physical width of the plasma along its laboratory propagation axis as a function of flight time from 9 to 30 μs. Figure 7 plots these results. With reference to the diameter of the initial illumination volume, we find that in 30 μs this measure of the plasma width approximately doubles.

The expansion rate of an ultracold plasma depends principally on the thermal energy of its electrons. Considerable effort in the field of atomic ultracold plasma research has focused on the determination of the electron temperature over the life of the plasma and its relation to plasma expansion [12,17–20]. For plasmas prepared above threshold, these measurements have generally supported the idea that the quantity, $T_e = 2E_e/3k_B$, reasonably describes the initial electron temperature so long as E_e, the excess energy, exceeds ~50 cm^{-1}. For plasmas produced by photoexcitation tuned lower in energy to release free electrons with less translational energy, and lower still to populate high-Rydberg states, electron heating mechanisms dominate to maintain

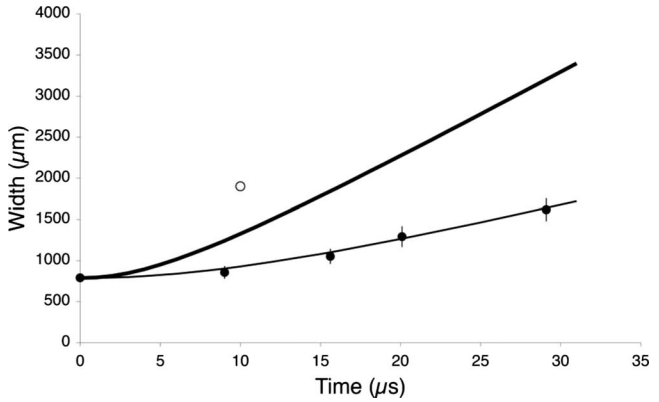

FIG. 7. Plot of plasma FWHM at G_2 as a function of flight time, compared with width predicted after 10 μs for ambipolar expansion at T_e=40 K (open dot) and Vlasov expansion of a spherical Gaussian plasma for $T_e(0)$=40 K (bold line). The line through the data represents a Vlasov fit for $T_e(0)$=6.8 K. Error bars reflect the experimental uncertainty in the measured flight distance to G_2, which exceeds the error introduced by using velocity averages to transform time to distance.

initial electron temperatures in the range of 40 K.

Direct photoionization, as well as Penning and electron-Rydberg collisional ionization form ions with an initial temperature largely unchanged from that of the neutral precursor. Momentum transfer from electrons is slow owing to the very large ion-electron mass difference. But ion-ion interactions can release potential energy by the mechanism of disorder-induced heating [21]. For a completely disordered initial system of ultracold ions interacting by means of the electron-screened repulsion of a Yukawa potential, molecular-dynamics simulations predict the ion temperature upon equilibrium to conform with

$$T_i = \frac{2}{3}\frac{e^2}{4\pi\epsilon_0 a k_B}\left|\frac{u}{\Gamma_i}+\frac{\kappa}{2}\right|, \tag{4}$$

where u/Γ_i is the electrostatic potential energy per particle in units of the average ion-ion repulsion energy. The sum of this term with $\kappa/2$, where κ is the ratio of the Wigner-Seitz radius, a, to the Debye length, λ_D, accounts for screening by the plasma electrons. Under conditions typical of atomic ultracold plasmas in MOTs, κ falls in the range of 0.5, $u/\Gamma_i \approx -0.7$, and disorder-induced heating gives rise to an equilibrium ion temperature between 1 and 2 K [22,23].

Under molecular-beam conditions, we prepare an initial population of NO Rydberg molecules with a translational temperature of about 1 K and a density in the range of 5×10^{12} cm^{-3}. Assuming complete avalanche ionization, this population evolves to form a plasma with a Wigner-Seitz radius of 360 nm. This average ion-ion distance is nearly an order-of-magnitude smaller than the value of a typically found in MOT plasmas, and reference to Eq. (4) might suggest the prospect of significant disorder-induced heating, and a substantial increase in ion temperature upon equilibration. Simple adjustment for smaller a, however, neglects the increasing effect of electron screening at higher charge density. Assuming an initial electron temperature of T_e=7 K (justified below), the initial Debye length under our conditions is λ_D=82 nm, yielding a κ of 4.4. Simulation results for an initial ion correlation of Γ_i=46 predict u/Γ_i=−2.29 [24], and an equilibrium ion temperature warmed by disorder-induced heating to only about 2 K.

Electrons released by plasma formation expand much more rapidly than the heavier positive ions. However, the attractive force of a developing space charge acts in constraining the expanding electron spatial distribution to grow no faster than the time scale for cation motion. By this Coulomb coupling, the thermal energy of the electrons drives overall plasma expansion, viz.:

$$\frac{1}{2}M_i v^2 = \frac{1}{2}k_B T_e. \tag{5}$$

For NO^+ in a plasma with an electron temperature of 40 K, this expression predicts an expansion rate of 100 μm μs^{-1}. An open dot on Fig. 7 shows the width after 10 μs predicted by Eq. (5) for a plasma with an initial diameter, $\sigma(0)$=758 μm. Clearly, the size expected for ambipolar expansion at $T_e(0)$=40 K substantially exceeds our observations. But we should expect this simple picture to overestimate the expansion rate. By expanding, the electron charge distribution does work on the cations so the temperature of the system, and thus the force driving its expansion, should fall with time.

A fuller account of the coupled evolution of the particle density and energy distribution functions is provided by the Vlasov equations [25], which form the foundation of the kinetic theory of plasmas, and have analytical forms for many types of low-density collisionless plasmas [26]. Laha and co-workers [12] have applied an analytical self-similar solution to describe the expansion of a quasineutral ultracold plasma configured to have a spherically symmetric Gaussian ion-density distribution. The evolution time scale for such a plasma is given by

$$\tau_{\rm exp} = \sqrt{\frac{m_i\sigma(0)^2}{k_B[T_e(0)+T_i(0)]}}, \tag{6}$$

where the quantities denoted as $T_\alpha(0)$ refer to the initial temperature of the electrons, $T_e(0)$, and the ions, $T_i(0)$. m_i is the mass of the ions.

The electron and ion temperatures fall with time according to

$$T_\alpha(t) = \frac{T_\alpha(0)}{1+\dfrac{t^2}{\tau_{\rm exp}^2}}, \tag{7}$$

and the diameter of the plasma expands as

$$\sigma(t) = \sqrt{\sigma(0)^2[1+t^2/\tau_{\rm exp}^2]}. \tag{8}$$

This simple formalism conforms very well with experimental measurements of ion positions and correlated expansion velocities in quasineutral ultracold plasmas of strontium prepared to have electron temperatures in the range of $T_e(0)$=40 K and above [12].

For reference, the bold line on Fig. 7 gives the time-dependent width predicted by Eq. (8) for a plasma with the ion mass of NO, an initial width of 785 μm, and initial electron and ion temperatures of $T_e(0)=40$ K and $T_i(0)=2$ K. The curve shown significantly overestimates the rate at which our plasma expands.

The collimated laser-crossed molecular-beam excitation geometry of our experiment produces a prolate ellipsoidal plasma volume, as opposed to a Gaussian sphere. Nevertheless, beam profiling shows that our laser intensity distribution in the yz plane is Gaussian, and slice measurements of the electron signal along the molecular-beam propagation axis show that this distribution of excitation intensity gives rise to a Gaussian plasma density distribution in the equatorial dimension.

Experiments by Cummings *et al.* [5] form an ellipsoidal plasma volume of similar aspect ratio in a calcium MOT. They determine an equatorial expansion rate by modeling the time-dependent Ca^+ laser-induced fluorescence signal. Although the analytical self-similar solution of the Vlasov equations for a spherically symmetric Gaussian plasma do not extend to this geometry, the expansion rate deduced by Cummings *et al.* [5] for calcium accords almost exactly with that found experimentally for the spherical strontium plasma of Laha *et al.* [12] when matched for initial electron energy and scaled to account for the ion mass difference.

This suggests that a simple fit of the spherical formalism to the rate of expansion in the equatorial dimension provides a reasonable gauge of electron temperature for Gaussian ellipsoidal plasma geometries.

The line drawn through the data on Fig. 7 represents a Vlasov fit to the equatorial plasma diameters measured in our experiment, returning an initial electron temperature of $T_e(0)=6.8$ K [for an assumed ion temperature of $T_i(0)=2$ K]. Remarkably, by this fit, the Vlasov equations hold that after 30 μs the electron temperature of our plasma has fallen to 1.4 K. By this point, plasma expansion has doubled the Wigner-Seitz radius but the predicted electron correlation remains substantial, $\Gamma_e \approx 10$.

This plasma forms following nitric oxide Rydberg-Rydberg Penning ionization collisions. Some initially formed electrons leave the excitation volume immediately, creating an electrostatic trap in which an electron-NO^* avalanche ionizes the remaining Rydberg molecules. Pohl and co-workers have recognized the collisional ionization of Rydberg atoms as a cooling mechanism for electrons in ultracold plasmas [27]. MOT experiments appear to show that the properties of atomic ultracold plasmas vary continuously with excitation energy tuned across the ionization threshold (c.f. Fig. 5 in Ref. [5]). Thus, we expect the plasma formed from Rydberg NO molecules to exhibit a relatively low electron temperature.

However, as mentioned above, efficient heating mechanisms appear to elevate electron temperatures, even in systems prepared very near the threshold, to levels much higher than seem to be evident here. Chief among these for the lowest initial values of T_e is three-body recombination [19].

In simple physical terms, three-body recombination occurs when an electron approaches an ion to within a critical radius, r_T, during which time a collision with a second electron carries away the binding energy of the pair. By this mechanism, any ion-electron collision resonance bound at least by the energy to which the electron collisionally thermalizes can remain bound. Thus, T_e determines the largest orbital radius stabilized by three-body recombination (the Thomson radius [28]) by the energy balance:

$$\frac{3}{2}k_B T_e = \frac{e^2}{4\pi\epsilon_0 r_T}. \tag{9}$$

This largest diameter least-bound orbital dominates recombination by virtue of the cross sections for electron capture and collisional thermalization, which scale as r^2. Thus, the rate of three-body recombination vastly accelerates as the electron temperature approaches 0 K. Various collision theory formulations developed to model three-body recombination consistently yield third-order rate constants that scale with temperature as $T_e^{-4.5}$ [29,28,30–32]. Calculations for ultracold atomic plasmas show that three-body recombination makes it difficult to form a plasma with an electron temperature less than 25 K [20].

The very high rates predicted for low-temperature three-body recombination follow directly from the very large values of r_T sampled in theory by low-energy recombining and deactivating electrons, or equivalently, the very high values of maximum principal quantum number, n_{max} (and accompanying orbital degeneracy), set by temperature in detailed-balance integrals.

However, conventional formulations of the three-body recombination rate neglect the effect of plasma density on the accessible scale of r_T or n_{max}. For an electron temperature, $T_e=2$ K, the average kinetic energy, 2.6 meV, dictates a Thomson radius of 560 nm. For a typical MOT plasma with a density of 3×10^{15} m^{-3}, this lies well within the Wigner-Seitz radius of 4 μm. By contrast, we estimate the plasma formed under our molecular-beam conditions to have an ion density of 5×10^{18} m^{-3}, or a Wigner-Seitz radius of 360 nm. Models incorporating the effects of ion density on high-n capture yield predicted rate coefficients that scale as T_e^{-1}, significantly reducing the predicted rate of three-body recombination [33,34].

Thus, it appears that conditions are right in our beam experiment to suppress three-body recombination and its attendant electron heating effects, diminishing the rate of plasma expansion in comparison with atomic systems prepared in MOTs.

A suppression of ion-electron recombination seems also apparent in the absence of dissociative recombination. We have noted previously [13] that a plasma lifetime of 9 μs exceeds expectations based on known cross sections for the dissociative recombination of NO^+ [35]. Present results include NO^+ plasmas that maintain a high degree of integrity for as long as 30 μs.

Among the factors that regulate ion and electron temperatures in molecular-beam plasmas, we might also consider the effect of the neutral carrier gas, which forms a background that is 100 fold more dense than the charged particles. In order to study the extent of plasma expansion following flight times from 8 to 30 μs, we vary the composition of this

background from 4 amu He to 84 amu Kr. Neglecting this difference ignores possible variations in density and temperature of the NO beam with carrier gas, and possible variations in the temperatures of subsequently formed ions and electrons owing to different thermalizing interactions with this background.

Supersonic expansion dynamics within the limit of an ideal monoatomic gas predict the same density and translational temperature regardless of the atomic mass of the carrier [14,15]. Nonideal effects include the formation of rare-gas dimers. This is known to occur to a significant degree for Xe, and consequent heating appears to suppress plasma formation in our experiment. For the remaining carrier gases from He to Kr, we find NO cooled to the same rotational temperature, $T_R^\infty = 2.5$ K, which provides experimental grounds to suppose translational cooling to comparable values of $T_\parallel^\infty$.

Once the plasma forms, the background gas constitutes a thermal reservoir for its charged particles. As the local temperature of this reservoir is little different from the estimated equilibrium temperatures of the ions and electrons, differential exchanges in energy exchange as a function of rare gas would be hard to detect. In any event, such processes would occur slowly on our time scale because the gas kinetic collision frequency under our molecular-beam conditions of density and temperature is no more than 2×10^5 s^{-1}. Cross sections for momentum transfer by elastic electron-atom collisions vary widely for the rare gases from He to Kr but one can expect the absolute rate for all gases to be slow on a microsecond time scale because of the inefficiency of mass-mismatched collisions.

Separate measurements of the plasma expansion rate for each of these rare-gas carriers would immediately reveal whether collisions with this background differentially affect the properties of this $NO^+ - e^-$ plasma. We are presently building a molecular-beam time-of-flight apparatus with a moveable detection grid for the purpose of making these measurements.

ACKNOWLEDGMENTS

It is a pleasure to acknowledge helpful discussions with T. Gallagher, D. Luckhaus, T. Pohl, and J. M. Rost. This work was supported by the Natural Sciences and Engineering Research Council of Canada (NSERC), the Canada Foundation for Innovation (CFI), and the British Columbia Knowledge Development Fund (BCKDF).

[1] M. P. Robinson, B. Laburthe Tolra, M. W. Noel, T. F. Gallagher, and P. Pillet, Phys. Rev. Lett. **85**, 4466 (2000).
[2] S. K. Dutta, D. Feldbaum, A. Walz-Flannigan, J. R. Guest, and G. Raithel, Phys. Rev. Lett. **86**, 3993 (2001).
[3] T. Gallagher, P. Pillet, M. Robinson, B. Laburthe-Tolra, and M. W. Noel, J. Opt. Soc. Am. B **20**, 1091 (2003).
[4] W. Li *et al.*, Phys. Rev. A **70**, 042713 (2004).
[5] E. A. Cummings, J. E. Daily, D. S. Durfee, and S. D. Bergeson, Phys. Plasmas **12**, 123501 (2005).
[6] T. Amthor, M. Reetz-Lamour, S. Westermann, J. Denskat, and M. Weidemüller, Phys. Rev. Lett. **98**, 023004 (2007).
[7] T. Killian, Science **316**, 705 (2007).
[8] T. Killian, T. Pattard, T. Pohl, and J. Rost, Phys. Rep. **449**, 77 (2007).
[9] S. Rolston, Physics **1**, 2 (2008).
[10] S. Ichimaru, Rev. Mod. Phys. **54**, 1017 (1982).
[11] G. Vitrant, J. Raimond, M. Gross, and S. Haroche, J. Phys. B **15**, 49 (1982).
[12] S. Laha, P. Gupta, C. E. Simien, H. Gao, J. Castro, T. Pohl, and T. C. Killian, Phys. Rev. Lett. **99**, 155001 (2007).
[13] J. P. Morrison, C. J. Rennick, J. S. Keller, and E. R. Grant, Phys. Rev. Lett. **101**, 205005 (2008).
[14] D. R. Miller, *Atomic and Molecular Beam Methods* (Oxford University Press, New York, 1988), pp. 14–53.
[15] H. Beijerinck and N. Verster, Physica B & C **111**, 327 (1981).
[16] M. Vrakking and Y. Lee, J. Chem. Phys. **102**, 8818 (1995).
[17] J. L. Roberts, C. D. Fertig, M. J. Lim, and S. L. Rolston, Phys. Rev. Lett. **92**, 253003 (2004).
[18] P. Gupta, S. Laha, C. E. Simien, H. Gao, J. Castro, and T. C. Killian, Phys. Rev. Lett. **99**, 075005 (2007).
[19] R. S. Fletcher, X. L. Zhang, and S. L. Rolston, Phys. Rev. Lett. **99**, 145001 (2007).
[20] F. Robicheaux and J. D. Hanson, Phys. Rev. Lett. **88**, 055002 (2002).
[21] M. S. Murillo, Phys. Rev. Lett. **87**, 115003 (2001).
[22] C. E. Simien, Y. C. Chen, P. Gupta, S. Laha, Y. N. Martinez, P. G. Mickelson, S. B. Nagel, and T. C. Killian, Phys. Rev. Lett. **92**, 143001 (2004).
[23] Y. C. Chen, C. E. Simien, S. Laha, P. Gupta, Y. N. Martinez, P. G. Mickelson, S. B. Nagel, and T. C. Killian, Phys. Rev. Lett. **93**, 265003 (2004).
[24] S. Hamaguchi, R. T. Farouki, and D. H. E. Dubin, Phys. Rev. E **56**, 4671 (1997).
[25] G. Manfredi, S. Mola, and M. Feix, Phys. Fluids B **5**, 388 (1993).
[26] D. S. Dorozhkina and V. E. Semenov, Phys. Rev. Lett. **81**, 2691 (1998).
[27] T. Pohl, D. Comparat, N. Zahzam, T. Vogt, P. Pillet, and T. Pattard, Eur. Phys. J. D **40**, 45 (2006).
[28] D. R. Bates and S. P. Khare, Proc. Phys. Soc. London **85**, 231 (1965).
[29] B. Makin, Phys. Rev. Lett. **11**, 281 (1963).
[30] S. G. Kuzmin and T. M. O'neil, Phys. Plasmas **9**, 3743 (2002).
[31] P. Mansbach and J. Keck, Phys. Rev. **181**, 275 (1969).
[32] M. R. Flannery and D. Vrinceanu, in *Atomic Processes in Plasmas*, AIP Conf. Proc. No. 443 (AIP, New York, 1998), p. 317.
[33] Y. Hahn, Phys. Lett. A **231**, 82 (1997).
[34] Y. Hahn, Phys. Lett. A **264**, 465 (2000).
[35] I. F. Schneider, I. Rabadán, L. Carata, L. H. Andersen, A. Suzor-Weiner, and J. Tennyson, J. Phys. B **33**, 4849 (2000).